Title
Investigating methane hydrate in sediments using X-ray computed tomography

Authors
Freifeld, Barry M.
Kneafsey, Timothy J.

Publication Date
2004

Investigating Methane Hydrate in Sediments using X-Ray Computed Tomography

*Barry M. Freifeld and Timothy J. Kneafsey

Lawrence Berkeley National Laboratory
One Cyclotron Road, Berkeley CA 94720, USA,
bmfreifeld@lbl.gov

Keywords: gas hydrate, x-ray tomography, core imaging, hydrate kinetics

Abstract
A portable x-ray computed tomography (CT) system constructed for imaging core at drill sites has been used to characterize methane hydrate within porous media. A series of experiments have been performed using synthetic methane hydrate in a sand matrix, demonstrating the capabilities of x-ray CT imaging to spatially and temporally track hydrate dissociation. The method is demonstrated to be sufficiently sensitive to image and measure density changes in millimeter-sized nodules of hydrate in full-size (75 millimeter whole-round) core. Portability of the imaging system is significant because it allows for field deployment of the measurement system, thus avoiding the difficulties and uncertainties associated with preservation, storage, and transport of methane-hydrate-bearing samples. Determining the CT system's sensitivity to changes in hydrate saturation was a goal in conducting these experiments. Confidence intervals for estimating hydrate saturation changes have been established based upon the volume of the region of interest. For a hydrate nodule as small as a few millimeters in diameter, dissociation of 10% of the contained methane can be discerned.

Introduction

Thermal and kinetic properties of naturally occurring hydrates are important to evaluate whether a hydrate deposit can be exploited as an economic resource [1]. Investigation of hydrate in sediment samples has been performed using visual and microscopic examination [2], x-ray diffraction [3], Raman spectroscopic methods [4], and x-ray computed tomography (CT) [5][6]. The most common experimental method employed to investigate hydrate kinetics consists of measuring gas production (or uptake) from a dissociating (forming) hydrate sample, while monitoring sample pressure and temperature [7][8][9]. By starting with hydrates of known grain size, researchers have developed kinetic models of hydrate dissociation based upon assumptions of hydrate grain geometry. Unfortunately, batch experiments reveal little about processes as they occur within heterogeneous, natural samples. To understand the influence that the sediment matrix has on entrained hydrate, researchers require a nondestructive technique to visualize hydrate processes within the sample.

Using a medical x-ray CT scanner, Mikami et al. [5] showed dissociation occurring in an unlithified sand sample containing natural hydrate that was retrieved from the Mallik 2L-38 gas hydrate research well. This work was significant because it demonstrated the ability for x-ray CT to spatially and temporally track hydrate dissociation. Gas production was measured using a gas flow meter. Freifeld et al. [6] used a medical scanner to track an advancing dissociation front created by thermal stimulation of a synthetic hydrate/sand mixture. This work compared the amount of gas evolved with the observed spatial progression of the dissociation front through a cylindrical sample. The location of the hydrate dissociation front was compared to a simple moving boundary model that incorporated the latent heat of dissociation. The effective thermal conductivity of the hydrate/sediment mixture was estimated based upon the velocity of the phase change boundary.

The purpose of this paper is to describe a series of experiments performed using a portable x-ray CT system to quantify the dissociation process in a synthetic methane hydrate-sand system. It differs significantly from previous work, demonstrating the use of the CT system to estimate the quantity of hydrate dissociated with high spatial resolution, independent of pressure or gas flow-rate measurements. Gas production is still used to quantify the total amount of hydrate contained within the sample, but this measurement is independent of the CT system's independent determination of the percentage of hydrate dissociated both spatially and temporally throughout the sample. Tracking dissociation with detailed spatial information is important for understanding (at a macroscopic level) the influence hydrate/sediment textural fabric has on the hydrate dissociation process. Such tracking can also answer important questions about whether dissociation is a kinetic or equilibrium process. Portability of the x-ray CT scanner is significant because it allows for hydrate dissociation experiments to be performed at the location of core recovery. This overcomes the difficulty of having to preserve the hydrates at high pressures and low temperatures for transportation to a remote laboratory.

X-ray Imaging System

The geometry and layout of the portable x-ray CT system are shown in Figure 1 [10]. The most significant advantage of this system over the more commonly used medical style CT scanners, which typically scan 1 slice at a time, is that a 10 cm volume of core can be imaged simultaneously at high resolution. This is important for imaging transient processes, such as hydrate dissociation, since it allows rapid imaging of a large volume.

To obtain complete volumetric information, we perform a computer reconstruction on 180 radiographic images, acquired using a two degree rotation of the core between each image. The resulting volumetric data set consists of an x-ray attenuation assigned to each 200 μm voxel, or volume element. By calibrating to known standards, we can convert attenuation to density. To accurately discern small changes, we employ the technique of differential imaging, whereby all images acquired are subtracted from a baseline image set.

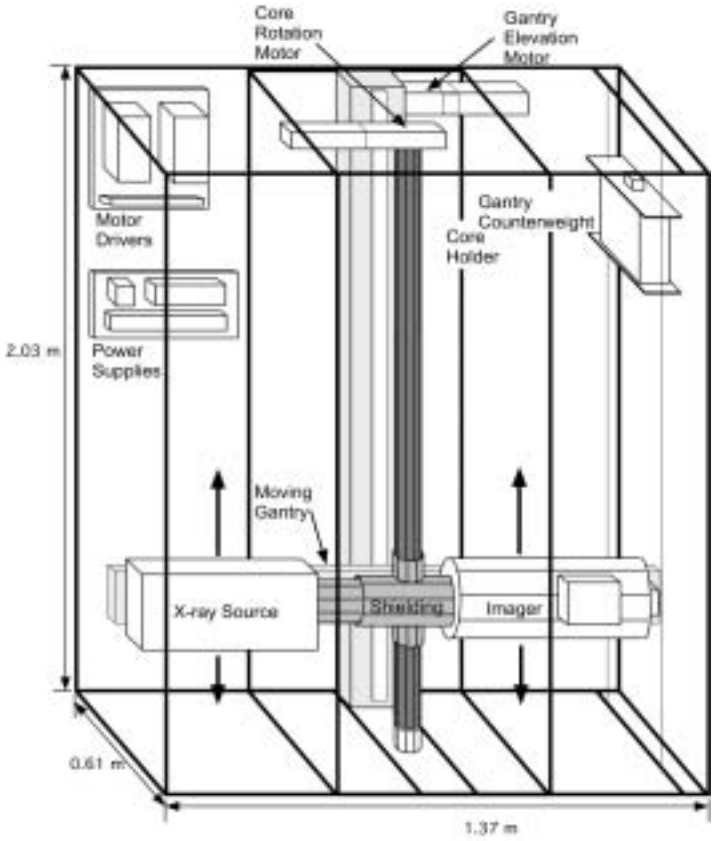

Figure 1. A schematic layout of the portable x-ray CT unit

For the experiments presented here, the beam energy was set at 130 kV and 200 μA. Because the x-ray beam is polychromatic, it will undergo beam-hardening as it transverses the sample, and soft x-rays will be more attenuated, yielding a beam containing a steadily higher proportion of harder x-rays. Without being corrected, beam-hardening makes the center of the sample appear denser than the outer edges. To reduce beam-hardening aberrations, we placed a 1.6 mm thick copper between the x-ray beam and the sample being imaged. The reconstructed image is post-processed using a polynomial correction to remove beam-hardening artifacts that the copper filter does not eliminate.

Methane Hydrate Dissociation Experiments

Methane hydrate dissociation experiments were performed using cylindrical synthetic porous methane hydrate samples. For brevity, two of them will be shown here. The 28.6 mm diameter cylinder of synthetic, 30%-porosity hydrate was fabricated by the USGS in Menlo Park, California by the process detailed in Stern et al. [3]. To preserve the hydrate and prevent dissociation, the hydrate was initially stored in a refrigerator at -80°C and then transported in a liquid nitrogen (LN) dry shipping dewar to Berkeley Lab.

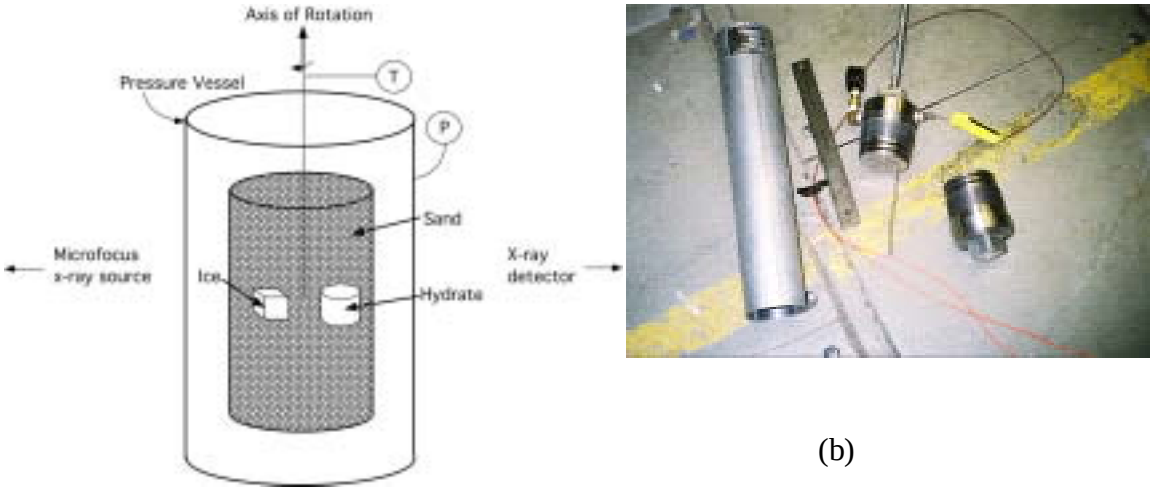

(a) (b)

Figure 2. (a) Schematic of hydrate experiment and (b) the pressure vessel used to hold the hydrate sample during CT scanning, showing the thermocouple wires and pressure gage on the top end cap

In each of the experiments, synthetic hydrate was added to a matrix of 12/20 mesh Ottawa sand. To prevent hydrate dissociation while preparing the sample at atmospheric pressure, we cooled the sand and hydrate using LN. Ice made from de-aired water and cooled with LN was used as a reference material. The ice provides a stable reference material because of its low porosity, only influenced by thermal expansion as it warms. The unconsolidated sand is susceptible to thermal-mechanical effects and changes in the density of the gas in the pore space as the sample warms and hydrate dissociates. Early in the experiment, the apparent density of the unconsolidated sand will be influenced by LN evaporation and the release of sorbed nitrogen.

The sand, hydrate, and ice samples were placed in a high-density polyethylene bottle (7.0 cm diameter × 12.7 cm high) and placed in an aluminum pressure vessel for imaging. Figure 2(a) shows an idealized schematic of the experimental set up, and Figure 2(b) shows a photograph of the pressure vessel used to hold the sample during x-ray CT scanning. The actual geometry of the hydrate and ice contained within the samples are shown in the reconstructed CT images.

The pressure in the closed vessel was monitored using a pressure gage to track the amount of hydrate dissociated. A thermocouple installed near the center of the sand/hydrate mixture provided a local indication of sample temperature. The exact thermal profile within the pressure vessel was unknown. However, the temperature as reported lagged the average temperature of the sample, which lay close to the temperature

indicated by the thermocouple, but somewhere between the indicated temperature and room temperature. This was clearly the case, because the pressure in the vessel increased, indicating hydrate dissociation, prior to the indicated temperature rising above the hydrate stability temperature (-76°C at 0.1 MPa).

Dissociation was induced by allowing the sample to warm through the stability point using room heat. Temperature and pressure were recorded using a thermocouple with a digital readout and a borden tube pressure gage. Acquiring a set of 180 CT radiographs took 3 minutes, and was performed approximately every 10 minutes. (The experiment conditions are presented in Table 1.) The Feldkamp reconstruction algorithm was applied to the radiographic data to give volume density information. For each reconstructed data set, a file containing 430 × 430 × 400 voxels was created, each element representing the density of a 200 μm cubical volume element.

First Experiment

The first dissociation experiment used a 32 mm long section of the 28.6 mm diameter porous hydrate sample. A cube of water ice made from de-aired water was used as a reference material. Figure 3 shows vertical and horizontal cross sections from reconstructed CT images, revealing the layout of the sample. The thermocouple junction is located at the tip of the temperature probe in the sand close to the water ice. Measured pressure and temperature are plotted in Figure 4(a). The time indicated is referenced to the time the baseline set of CT images were acquired. The pressure rise that occurs prior to acquisition of the baseline image set is due to the boiling of residual LN in the sample. When the pressure in the vessel stopped increasing (at about 40 minutes), dissociation was considered complete. Figure 5 shows a horizontal slice taken through the hydrate cylinder in the sand matrix, along with difference images calculated by subtracting later images from the baseline image. The bright spot near the hydrate is caused by the stainless steel sheath around the thermocouple wires.

Second Experiment

The second dissociation experiment used a 19 mm long section of the 28.6 mm diameter hydrate. Prior to mixing with sand, the hydrate was broken into several pieces of assorted sizes. The smallest clearly discernable hydrate piece was approximately 2.4 mm × 3.2 mm × 4.8 mm, having a total volume of about 0.037 cm^3. Similar to Experiment 1, a cube of ice was used as a reference standard. Figure 4(b) shows measured pressures and temperatures. Figure 6 shows a horizontal slice taken through the sample, with the baseline image revealing various nodules of hydrate and the one large water ice piece. The difference images were calculated by subtracting subsequent images from the baseline image.

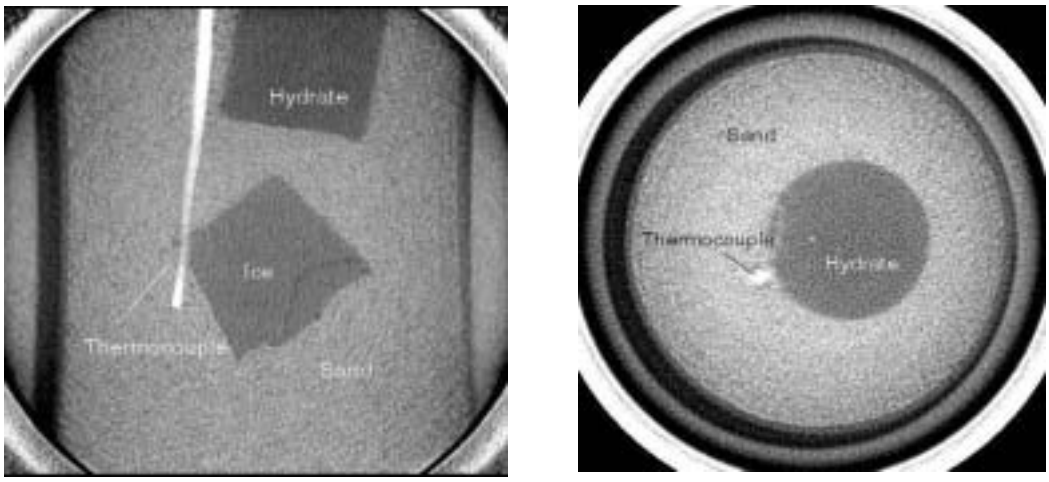

(a) (b)

Figure 3. (a) Vertical and (b) horizontal cross sections taken during Experiment 1, revealing hydrate and ice in a sand matrix

Table 1. Experiment conditions

Experiment	Hydrate Geometry	Hydrate Volume (cm^3)	Moles Methane	Estimated Methane Evolved (moles)
1	Cylindrical segment	20.4	0.12	0.13
2	Nodules	12.2	0.074	0.053

Discussion

Pressure and Temperature Data

The pressure and temperature data recorded for each experiment are presented in Figure 4. Table 1 shows the estimated moles of methane gas evolved calculated using the measured increase in gas pressure and the gas-filled volume of the pressure vessel. Both experiments show increases in pressure prior to when the temperature of the sample was above the dissociation temperature for the hydrate. This early rise is due to the nitrogen boiling off. The subsequent increases in pressure were due to hydrate dissociation. The evolved gas volume, estimated using the ideal gas law, roughly matches the known volume initially contained by hydrate for these two experiments.

CT Data

CT data were collected periodically during the dissociation experiments. Figures 5 and Figure 6 show a baseline image and difference images for Experiment 1 and Experiment 2, respectively. Significant reductions in hydrate density were observed during dissociation, whereas only minor changes in the density of ice and the bulk density of

sand were observed. The percent hydrate dissociated for each experiment was estimated using the measured attenuation data from a volume of interest in the interior of the hydrate and plotted along with temperature and pressure on Figure 4. These regions are highlighted on the last difference image shown for each experiment. The volume of interest for Experiment 1 was a central region of the cylindrical hydrate sample. For Experiment 2, which contained many small hydrate nodules, the percent dissociated was based upon an average of three different interior volumes. To convert from x-ray attenuation to density, a calibration used the measured x-ray attenuation from the baseline image for the known materials: sand, hydrate and water ice.

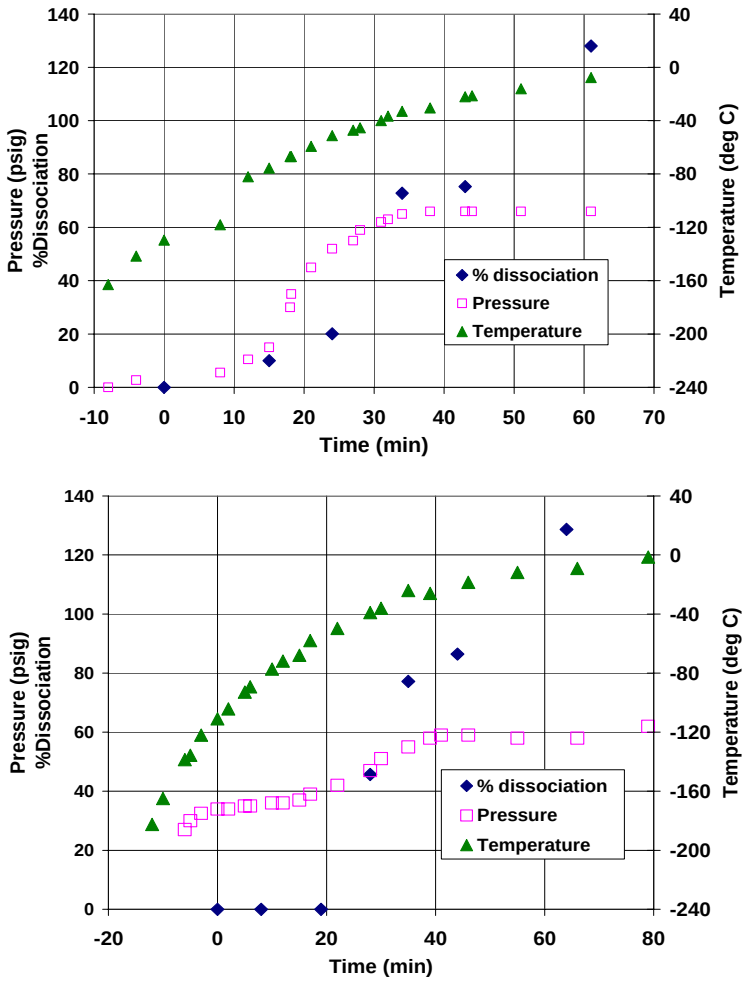

Figure 4. Pressure, temperature, and percent hydrate dissociated, as estimated from x-ray CT images, for (a) Experiment 1 and (b) Experiment 2

Difference images from Experiment 1 (Figure 5) show the dissociation of a single large cylinder of hydrate. A small halo at the edge of the cylinder first appears in the difference image acquired 15 minutes after baseline. Dissociation progresses inward. The image at 24 minutes shows a continuous ring of dissociated hydrate at the edge of the cylinder with more pronounced dissociation at the warmest area, the edge closest to the pressure vessel wall. At 34 minutes, dissociation has occurred throughout the entire volume of the hydrate, with only a slight change noticeable at 43 minutes. The final image, at 61 minutes, reveals a drastic reduction in density at the edges of the hydrate cylinder and the estimated percent hydrate dissociated has jumped up to 130% of the theoretical value. This large reduction in density results from mechanical expansion of the sample. The bright ring around the final image shows the increase in volume of the original hydrate cylinder, now consisting of water ice.

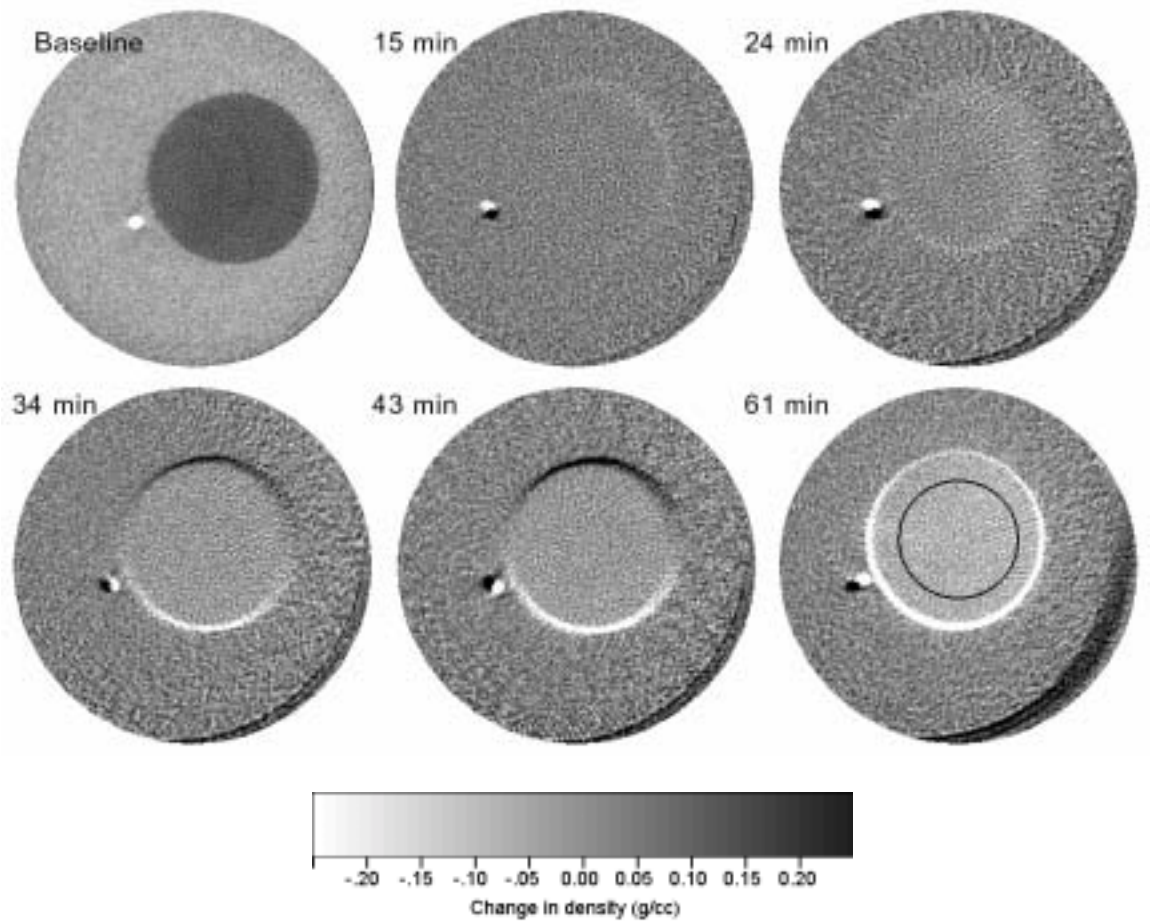

Figure 5. A sequence of horizontal images from Experiment 1. The baseline image shows the cylinder of hydrate surrounded by sand. All subsequent images are differences taken from the baseline image. Dissociation starts as a faint halo at the edge of the hydrate, steadily progressing throughout the hydrate. The black circle indicates the region of interest used to calculate the change in hydrate density. The greyscale legend applies only to the difference images

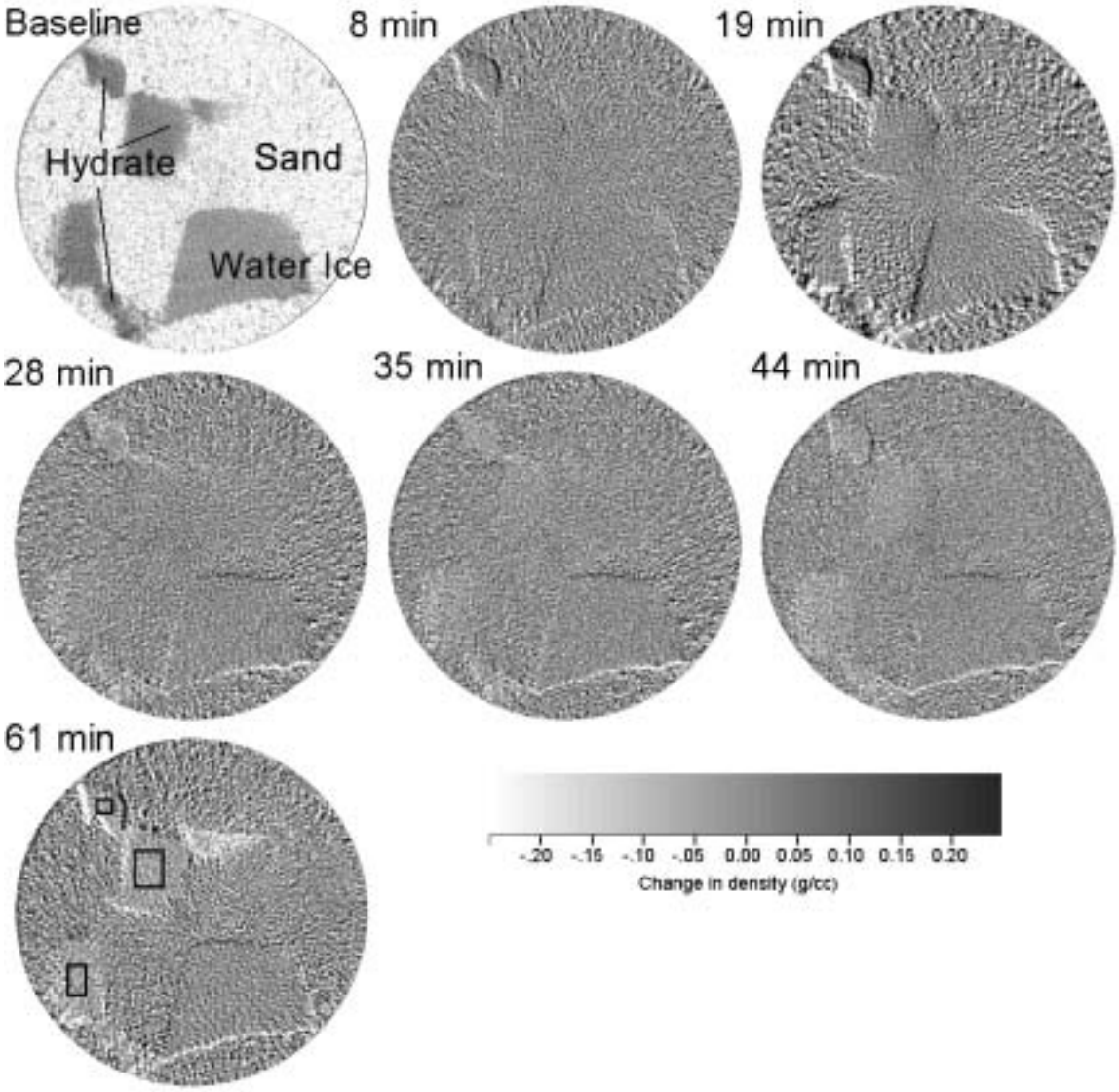

Figure 6. A sequence of horizontal slices from Experiment 2, showing both methane hydrate and water ice in a sand matrix. All images after baseline have been differenced with the baseline image. The rectangles in the last image (time 61 minutes) show the regions of interest used to calculate the change in hydrate density. The greyscale legend applies only to the difference images.

Difference images from Experiment 2 (Figure 6) show changes similar to those from Experiment 1. Dissociation occurs in the hydrate nodules earliest near the walls of the pressure vessel and progress inward. The image acquired at 28 minutes shows that the hydrate at the edge of the vessel has undergone significant reduction in density, whereas the interior hydrate nodules are unchanged. At 35 minutes, dissociation is visible

throughout the hydrate, becoming more pronounced at 44 minutes. The image acquired at 61 minutes shows a large density reduction (130% of the expected value for hydrate dissociation), again accompanied with apparent displacement of sand and expansion of the hydrate sample.

Experimental Uncertainty

There are numerous sources of noise, error, and uncertainty in the estimation of density from x-ray CT images. Some of these errors are systematic and arise from the reconstruction process, since the Feldkamp Algorithm that is used for processing the data is an approximate method. These can be corrected during postprocessing. Beam hardening is one of the largest sources of error in making accurate density estimates. To eliminate beam hardening beyond what is removed by passing the x-ray beam through a copper filter, the reconstructed data set is normalized using a polynomial that is a function of the distance from the rotational axis of the core sample. To perform this correction, we normalize the reconstructed image set by the reciprocal of the beam-hardening trend, fitted by a second order polynomial.

Other errors, such as camera noise, are Gaussian, and can be quantified using standard statistical analysis, so that confidence intervals can be determined for the density estimates. There is a significant amount of error in any one 200 μm cubical voxel. The 95% confidence interval for a density estimate can be expressed as:

$$\rho_{0.95}(x) = \rho(x) \pm t_{0.95,n} \frac{\sigma}{\sqrt{n}}$$

where n is the number of voxels, σ is the standard deviation of measured voxel densities, and t is Student's t distribution. The 95% confidence interval for estimating the density change for the water ice in Experiment 2 is shown in Figure 7(a) as a function of the length of a cubical region of interest. The density estimate as one approaches a region a few millimeters in length decreases to an uncertainty of approximately ±0.01 g/cc. For the ice shown, no change in density is expected. Similarly, confidence intervals for a region in the interior of a nodule of hydrate in Experiment 2 are shown in Figure 7(b) for each of the acquired image sets. Changes in hydrate saturation of 10% can easily be discerned for regions of hydrate greater than a few millimeters in diameter.

Conclusions

We have used x-ray computed tomography to determine the spatial distribution of hydrates in whole-round cores with high resolution. By repeatedly imaging the same section of core as dissociation occurs, hydrate kinetics can be investigated. Because the location of the dissociation front represents a region of known thermodynamic conditions, locating and tracking movement of the front provides information on rates of energy flux and mass transport. Estimation of density confidence intervals indicates that even relatively modest reductions in hydrate saturation can be accurately determined. Future studies will use the x-ray CT to measure hydrate kinetic parameters and determine thermal parameters of hydrate sediment systems.

(a)

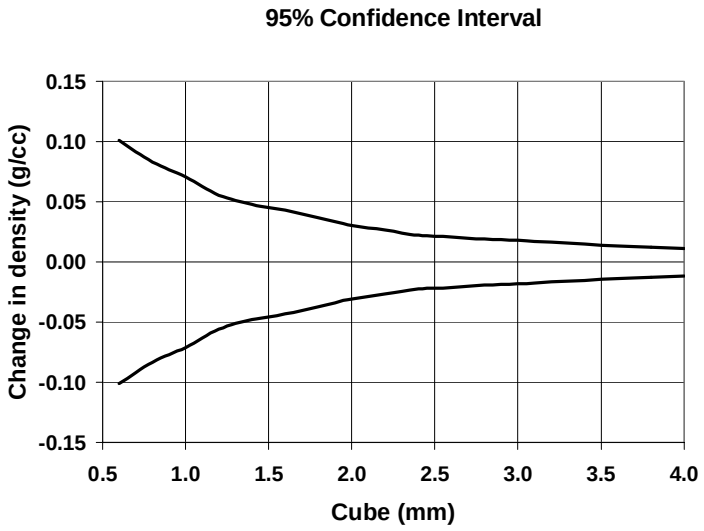

(b)

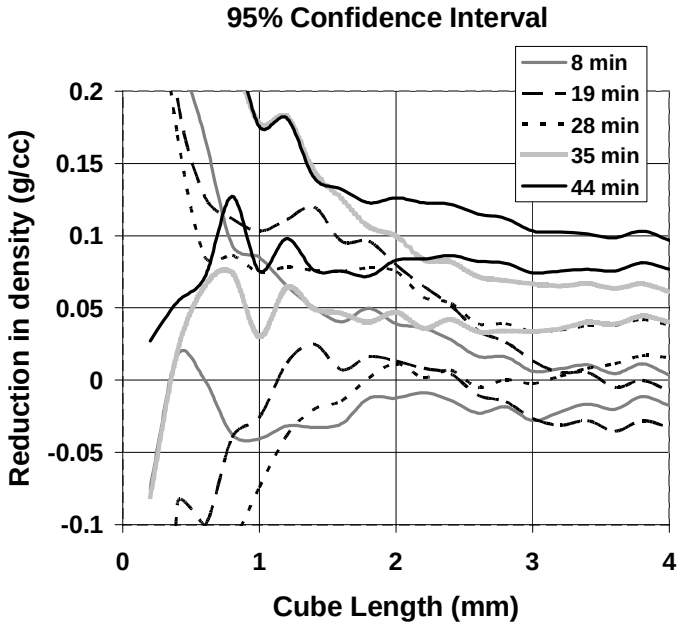

Figure 7. (a) The estimated change of density for the water ice in Experiment 2 with upper and lower 95% confidence intervals as a function of region size; (b) The reduction in hydrate density during dissociation. The density changes were estimated using attenuation data contained within a cubical region of hydrate in Experiment 2

Acknowledgments
This work was supported by the Assistant Secretary of the Office of Fossil Energy, Office of Natural Gas & Petroleum Technology, U.S. Department of Energy under Contract No. DE-AC03-76SF00098. The authors are grateful to Laura Stern from the USGS for supplying the synthetic methane hydrate sample used in this paper. The authors would also like to thank Dan Schneberk for making the CT image-processing code, Imgrec, available to us and Jacob Pruess for assistance in data analysis. In addition, we would like to thank Liviu Tomutsa and an anonymous reviewer for providing careful reviews of this manuscript.

References
(1) Moridis, G. J., Presented at SPE Gas Technology Symposium, Alberta, Canada. 2002, SPE 75691.
(2) Kobayashi, I.; Ito, Y.; and Mori, Y.H., *Chem. Eng. Sci.* 2001, 56; pp. 4331–4338.
(3) Stern, L. A.; Kirby, S. H.; and Durham, W. B.; *Science*, 1996, *273* (5283); pp. 1843–1848.
(4) Uchida, T.; Hirano, T; Ebinuma, T.; Narita, H.; Gohara, K.; Mae, S.; and Matsumoto, R., *AICHE Journal.* 1999, 45(12), 2641–2645.
(5) Mikami, J.; Masuda, Y.; Uchida, T.; Satoh, T.; and Takeda, H., In *Gas Hydrates, Challenges for the Future,* Annals of the New York Academy of Sciences, Volume 912., 2000; pp. 1011–1020.
(6) Freifeld, B. M.; Kneafsey, T. J.; Tomutsa, L.; Stern, L. A.; and Kirby S. H.; 2002, In *Proceedings of the Fourth International Conference on Gas Hydrates*, May 19–23, Chiba, Japan, 2002; pp. 750–755.
(7) Kim, H. C.; Bishnoi, P. R.; Heidemann, R. A.; and Rizvi, S. S. H.; Chem Eng. Sci., 1987, (42) 1645–1653.
(8) Clarke, M. A.; and Bishnoi P. R., *Can J. of Chem. Eng.* 2001, 79(1), 143–147.
(9) Circone, S.; Stern, L. A.; Kirby, S. H.; Pinkston, J. C., and Durham, W. B., In *Gas Hydrates, Challenges for the Future,* Annals of the New York Academy of Sciences, 2000, Volume 912; pp.544–555.
(10) Freifeld, B. M.; Kneafsey, T. J.; Tomutsa, L.; and Pruess, J.; 2003, In *Proceedings of the 2003 International Symposium of the Society of Core Analysts*, September 21–24 Pau, France. 2003; pp. 581–586.